Materials Science & Engineering A 622 (2015) 228–235

Contents lists available at ScienceDirect

Materials Science & Engineering A

journal homepage: www.elsevier.com/locate/msea

Effects of stress ratio on high-cycle and very-high-cycle fatigue behavior of a Ti–6Al–4V alloy

Xiaolong Liu, Chengqi Sun, Youshi Hong*

State Key Laboratory of Nonlinear Mechanics, Institute of Mechanics, Chinese Academy of Sciences, Beijing 100190, China

ARTICLE INFO

Article history:
Received 11 July 2014
Received in revised form
30 September 2014
Accepted 30 September 2014
Available online 7 October 2014

Keywords:
Ti–6Al–4V alloy
Stress ratio
Crack initiation type
Crack growth threshold
Very-high-cycle fatigue

ABSTRACT

The effects of stress ratio on high-cycle fatigue (HCF) and very-high-cycle fatigue (VHCF) behavior of a Ti–6Al–4V alloy were systematically investigated in this paper. Fatigue tests with ultrasonic frequency (20 kHz) were performed on specimens of a bimodal Ti–6Al–4V alloy with stress ratios of −1, −0.5, −0.1, 0.1 and 0.5. Three types of crack initiation mode were observed on the fracture surfaces of the specimens that failed in the HCF and the VHCF regimes, which were explicitly classified as surface-without-facets, surface-with-facets and interior-with-facets. With the increase of stress ratio from −1 to 0.5, the number of specimens for surface-without-facets decreased, that for surface-with-facets increased, and that for interior-with-facets increased first and then decreased. For the failure types of surface-with-facets and interior-with-facets, the fatigue strength decreased sharply in the VHCF regime, and the *S–N* curve switched from an asymptote shape to a duplex shape. Then, a new model based on Poisson defect distribution was proposed to describe the effects of stress ratio on the occurrence of different failure types, i.e., the competition of alternative failure types. The observations also showed that there is a rough area at the crack initiation region for interior initiation cases, and the values of the stress intensity factor range for the rough area are within a small range, with the mean value being close to the threshold for the crack starting to grow in vacuum environment of the alloy. The estimated value of plastic zone size at the periphery of rough area is close to the average diameter of the primary α grains of the alloy.

1. Introduction

Titanium alloys have been widely used as superior engineering materials because of their high specific strength, high temperature resistance and high corrosion resistance. In their engineering applications, such as in aircraft engines, titanium alloys may experience even 10^{10} fatigue cycles [1,2]. The fatigue behavior of titanium alloys in the very-high-cycle fatigue (VHCF) regime has drawn great attention in recent years. Neal and Blenkinsop [3] revealed that fatigue cracks initiated from the interior of the specimen with facet morphology of a Ti–6Al–4V alloy for the fatigue life exceeding 10^7 cycles at stress ratio (R) of zero, for which the nucleation of fatigue cracks was attributed to the cleavage of primary α grains. No pre-existing defects were observed at the initiation region for that case. A similar phenomenon was reported in other titanium alloys, such as Ti-6246 [4] and Ti–15Mo–5Zr–3Al [5]. Chandran et al. [6–9] investigated the effects of the volume fraction of primary α nodules on the preference of crack initiation types for a homogeneous titanium alloy Ti–10V–2Fe–3Al. They proposed a model based on a two-dimensional Poisson defect distribution to describe the competition of failure modes.

It is known that many factors, such as stress ratio [10–12], environment [13] and surface treatment [14–16], may affect fatigue crack initiation and propagation behavior of metallic alloys. As an important topic, the effects of stress ratio on fatigue crack initiation and propagation of titanium alloys were investigated in previous papers [17,18]. For $R=-1$, the results by Morrissey et al. [19] indicated that a Ti–6Al–4V alloy exhibited a fatigue limit and the *S–N* curve presented a continual downward shape in the high-cycle fatigue (HCF) and the VHCF regimes with crack initiation only from the specimen surface. No facet was found at the crack initiation region, and the mechanism for crack initiation was attributed to localized slip deformation. However, with the similar microstructure of the Ti–6Al–4V alloy, Zuo et al. [20] revealed that cracks initiated from the specimen's interior in the HCF and the VHCF regimes. Takeuchi et al. [21,22] invesigated the effects of frequency on the VHCF behavior of a Ti–6Al–4V alloy from three

* Corresponding author. Tel.: +86 10 82543966; fax: +86 10 62561284.
E-mail address: hongys@imech.ac.cn (Y. Hong).

http://dx.doi.org/10.1016/j.msea.2014.09.115
0921-5093/

factories with the same heat treatment. Their results showed that cracks initated from the surface for one of them and from both the surface and the interior for two of them. The reason for crack initiation from the surface or from both the surface and the interior at $R=-1$ is not clear. For the positive stress ratio, the results for a Ti–6Al–4V alloy [23,24] indicated that the fatigue strength exhibited a sharp decrease in the HCF and the VHCF regimes for the crack initiation from the interior with facets. It was also reported that cracks initiated occasionally from the surface with subsurface facets at the initiation region [25,26]. The formation of facets was due to the cleavage of primary α grains. Therefore, it is suggested that with the increase of stress ratio, an alternative failure mode of crack initiation is triggered, and the fatigue strength is decreased in the HCF and the VHCF regimes for the Ti–6Al–4V alloy.

The process of crack initiation consumes most of the fatigue life in the VHCF regime. For the VHCF of high-strength steels, more than 90% of fatigue life is consumed by the formation of the crack initiation region of fine granular area (FGA) [27]. Therefore, the mechanism of crack initiation and the competition among different mechanisms of crack initiation have attracted attention of researchers [9,28–30]. For example, Chandran [9] investigated the effects of the volume fraction of primary α nodules on the competition among crack initiation types for Ti–10V–2Fe–3Al alloys. Hong et al. [28] simulated the competition mechanism of fatigue crack initiation at the specimen surface or at the subsurface for high strength steels and concluded that large inclusion size, small grain size and high strength of the material promote the subsurface mode of crack initiation. Murakami [29] discussed the competition between surface defects initiation and interior inclusion initiation of steels, in which the crack initiation site was determined by the threshold value of the stress intensity factor range for surface defects and interior inclusion. Stanzl-Tschegg et al. [30] analyzed the proportion of surface and interior initiation of an aluminum–silicon alloy in the HCF and the VHCF regimes and indicated that the proportion of crack interior initiation in the VHCF regime is more than that in the HCF regime. However, the competition among different mechanisms of crack initiation for the Ti–6Al–4V alloy in the HCF and the VHCF regimes with the variation of stress ratio has not yet been studied.

For the case of crack initiation from the interior of the specimen, the morphology of rough area containing flat facets was observed at the crack initiation region for titanium alloys, which is similar to the FGA with rough surface at the interior initiation region of high-strength steels in the VHCF regime [31–33]. Shiozawa et al. [34] analyzed the effects of stress ratio on the value of the stress intensity factor range (SIF), which is calculated from the size of facets for a beta-type titanium alloy Ti–15V–3Cr–3Sn–3Al. The calculated value was smaller than the threshold for crack growth. Oguma et al. [24] also discussed the variation of SIF at the crack initiation region of a Ti–6Al–4V alloy. Indeed, the formation mechanism of rough area for titanium alloys is without in-depth investigation so far.

In this paper, a titanium alloy of Ti–6Al–4V was used for investigating the effects of stress ratio on the HCF and the VHCF behavior of the material. Fatigue tests were performed with an ultrasonic fatigue test machine, for which a mean stress is able to be superimposed. Stress ratios of -1, -0.5, -0.1, 0.1 and 0.5 were chosen, and relevant *S–N* curves were obtained. Three failure types of crack initiation, which were in relation with fatigue resistance, were explicitly identified on the fracture surfaces for the specimens that failed in the HCF and the VHCF regimes. A new model based on the Poisson defect distribution was developed to describe the competition of the failure types. In addition, the value of SIF and the size of the plastic zone for the rough area in the crack initiation region were calculated and discussed.

2. Test material and experimental methods

2.1. Test material

The material used in this investigation is an α–β titanium alloy (Ti–6Al–4V). The chemical compositions (mass percentage) are 5.8 Al, 4.2 V, 0.12 Fe, 0.03 N, 0.02 C, 0.005 H, 0.15 O and balance Ti. It was supplied as unidirectional rolled bars of 14 mm in diameter with equiaxed microstructures. A typical processing procedure (920 °C/1 h+air-cooling and 550 °C/4 h+air-cooling) was performed to produce bimodal microstructures consisting of equiaxed α grains and lamellar structure for the test material. The obtained microstructure is shown in Fig. 1. The microstructure is a homogeneous duplex pattern with about 50% volume fraction of primary α grains, and the remaining 50% is the lamellar structure of secondary α_s plates embedded in β matrix, which was taken from three microstructure photographs as shown in Fig. 1. The average diameter of primary α grains was measured as 5.89 μm by electron back-scattered diffraction with a measuring area of 200 μm × 200 μm.

Before performing fatigue experiments, the mechanical properties of the material were measured by tensile testing on an MTS 810 system with cylindrical specimens of 6 mm in diameter and at a strain rate of 10^{-4} s^{-1}. Five specimens were tested to obtain the yield strength of 812 MPa and the tensile strength of 945 MPa for the material. Microhardness measurement was performed with a Vickers hardness tester at a load of 50 g with the load holding time of 15 s. Twenty indentation points for each of the three specimens were performed. The average value of the hardness is 310 Hv.

2.2. Fatigue testing method

Fatigue testing was conducted on an ultrasonic fatigue test machine at a resonance frequency of 20 kHz at room temperature in air. The ultrasonic fatigue machine was equipped in a conventional tensile machine (capacity 20 kN) to enable the ultrasonic cycling under an amount of mean stress which was superimposed to each test of stress ratio of -0.5, -0.1, 0.1 or 0.5. Compressive air was used to cool the specimen during ultrasonic fatigue testing. The diameter of the minimum section for the specimen is 3 mm. For the case of $R=-1$, no mean stress was added, and the cyclic stress was solely loaded by the ultrasonic fatigue machine. For the stress ratio of -0.5, -0.1, 0.1 or 0.5, a value of mean stress was superimposed by the tensile machine. For the broken specimens, the fracture surfaces were examined by using a field-emission type of scanning electron microscope (SEM).

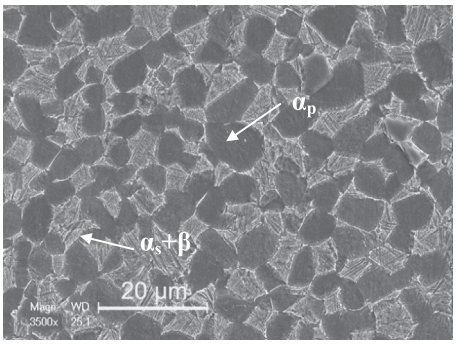

Fig. 1. Microstructure of the bimodal Ti–6Al–4V alloy (α_p: primary α grain, $\alpha_s+\beta$: lamellar structure).

3. Results

3.1. S–N curves

Fig. 2 shows the *S–N* curves for the Ti–6Al–4V specimens with stress ratios of −1, −0.5, −0.1, 0.1 and 0.5. There are two types of *S–N* curves shown in Fig. 2. For stress ratios of −1 and −0.5, the *S–N* curves present a horizontal asymptote shape and have a fatigue limit. For the stress ratios of −0.1, 0.1 and 0.5, the *S–N* curves present a step-wise or duplex shape, and the fatigue strength exhibited a sharp decrease in the VHCF regime. With the crack initiation type shown in Fig. 2, the sharp decrease in fatigue strength in the VHCF regime for the stress ratios of −0.1, 0.1 and 0.5 is evidently related to the fatigue crack initiation mechanism. With the increase of stress ratio, the case of surface crack initiation without subsurface facets disappeared and that of crack initiation with facets became dominant. Thus, the change of failure types of crack initiation probably resulted in the *S–N* curves switching from an asymptote shape to a duplex shape.

It is noted that with the increase of stress ratio, the tested stress range in terms of stress amplitude ($\Delta\sigma_{t,amp}$) decreases, and the tested stress range in terms of the maximum stress ($\Delta\sigma_{t,\,max}$) increases. As shown in Fig. 2(a), the value of $\Delta\sigma_{t,amp}$ at $R=-1$ is between 500 and 650 MPa, which is the superior consequence in fatigue resistance. While the value of $\Delta\sigma_{t,amp}$ at $R=0.5$ is between 150 and 250 MPa, which is the inferior consequence in fatigue resistance. Whereas in terms of the maximum stress as shown in Fig. 2(b), the tendency is reverse.

3.2. Fractography

Based on the SEM observations, three failure types of crack initiation mode were classified. Figs. 3, 4 and 5 show the fracture surfaces of such three failure types.

Type I: Crack initiation occurred from the surface without subsurface facets observed at the initiation region as shown in Fig. 3, which is named “surface-without-facets” for short. Fig. 3 (a) and (b) is the morphology of failed specimens with type I at low and high magnification. Fig. 3(c) presents the schematic of type I. No facet was presented in the initiation region. This kind of failure type is a common morphology for the fatigue failure of crack initiation for engineering alloys [19].

Type II: Crack initiation occurred from the surface with subsurface facets randomly distributed at the initiation region as shown in Fig. 4, which is named “surface-with-facets” for short. Fig. 4 (a) and (b) is the morphology of failed specimens with type II at low and high magnifications. Fig. 4(c) presents the schematic of type II. A couple of facets were arrowed in Fig. 4(b). The formation of facets is due to the cleavage of the primary α grains located in the subsurface region [25,26].

Type III: Crack initiation occurred from the specimen's interior with facets randomly distributed at the initiation region as shown in Fig. 5, which is named “interior-with-facets” for short. Fig. 5 (a) and (b) is the morphology of failed specimens with type III at low and high magnifications. Fig. 5(c) presents the schematic of type III. The outer boundary of the whole region for crack initiation and early growth sometimes exhibited a pattern of “fish-eye”,

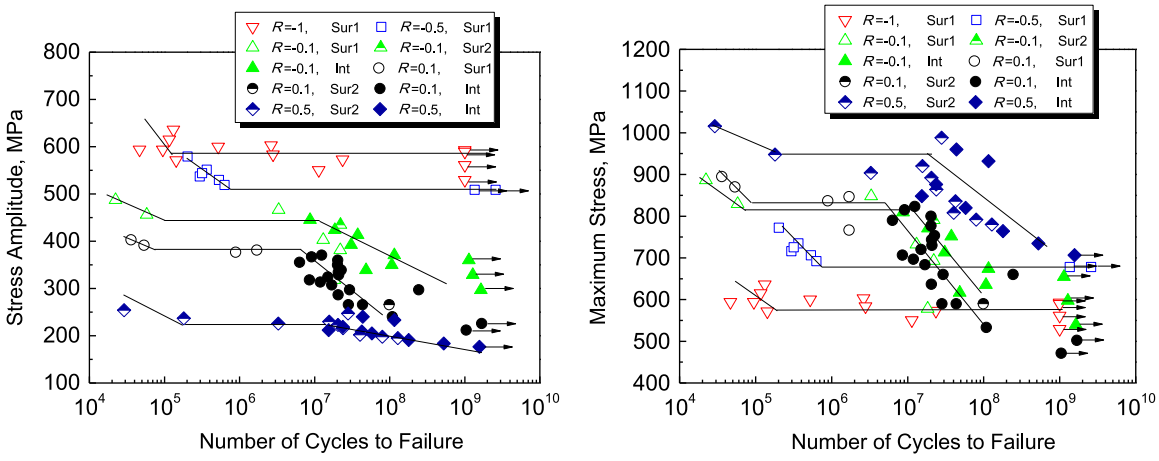

Fig. 2. *S–N* curves of the Ti–6Al–4V specimens with stress ratios of −1, −0.5, −0.1, 0.1 and 0.5. (a) In terms of stress amplitude and (b) in terms of the maximum stress (Sur1: surface-without-facets, Sur2: surface-with-facets, Int: interior-with-facets, symbol with arrow: no broken.).

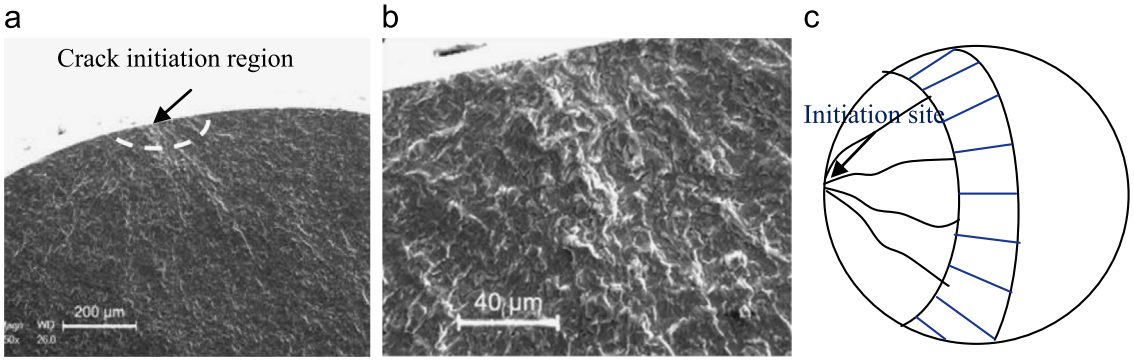

Fig. 3. Type I morphology “surface-without-facets” of failed specimens. (a) Low magnification image, (b) enlargement of initiation region, and (c) schematic presentation.

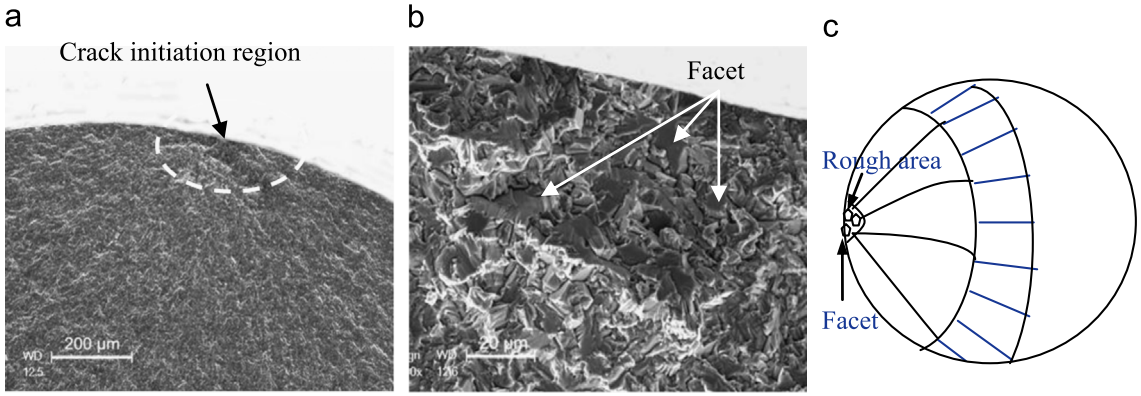

Fig. 4. Type II morphology "surface-with-facets" of failed specimens. (a) Low magnification image, (b) enlargement of initiation region, and (c) schematic presentation.

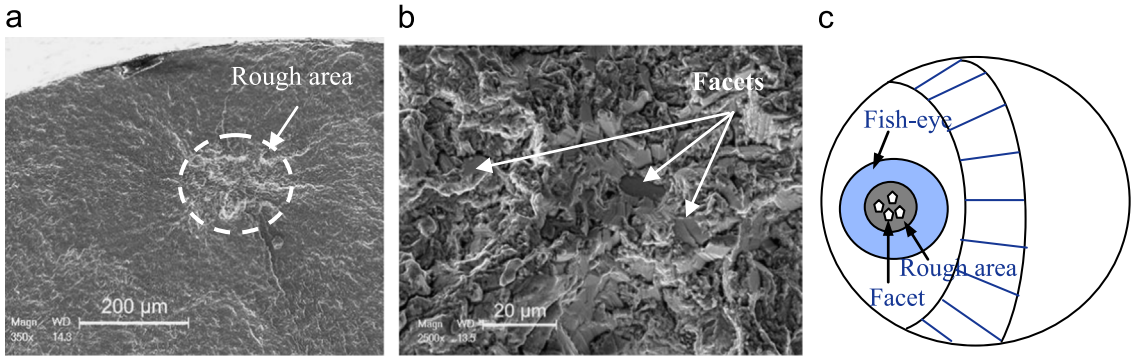

Fig. 5. Type III morphology "interior-with-facets" of failed specimens. (a) Low magnification image, (b) high magnification image, and (c) schematic presentation.

Table 1
The occurrence number and the fraction of failure type as a function of stress ratio [occurrence number (fraction)].

	$R=-1$	$R=-0.5$	$R=-0.1$	$R=0.1$	$R=0.5$
Surface-without-facets	10(100%)	6(100%)	4(36.4%)	0(0%)	0(0%)
Surface-with-facets	0(0%)	0(0%)	1(9.1%)	1(5.3%)	11(61.1%)
Interior-with-facets	0(0%)	0(0%)	6(54.5%)	18(94.7%)	7(38.9%)

which contains a clear feature of "rough area" as shown in Fig. 5(a). The rough area seems to be the crack initiation region. Within the rough area, a number of facets are always distributed as shown in Fig. 5(b). Facets were formed by the cleavage of the primary α grains, which was confirmed by EDS detection [3].

Table 1 presents the occurrence number and the fraction of each failure type in the HCF and the VHCF regimes with different stress ratios. The tendency is evident that with the increase of stress ratio, the number of specimens that failed from surface-without-facets decreases, the number of specimens that failed from surface-with-facets increases, and the number of specimens that failed from interior-with-facets increases first and then decreases. This indicates that there are competitions of the three failure types with the increase of stress ratio.

Fig. 6 shows two examples of surface-without-facets for the specimens at the stress ratios of −1 and −0.5. All such specimens including ten at $R=-1$ and six at $R=-0.5$ failed from surface-without-facets as shown in Table 1. No facet was observed in all such fracture surfaces.

For $R=-0.1$, eleven specimens in total failed in the HCF and the VHCF regimes. As listed in Table 1, four of them failed from surface-without-facets as shown in Fig. 7(a) and (b), one failed from surface-with-facets as shown in Fig. 7(c), and six of them failed from interior-with-facets as shown in Fig. 7(d).

For $R=0.1$, nineteen specimens in total failed in the HCF and the VHCF regimes. As listed in Table 1, one failed from surface-with-facets and the rest failed from interior-with-facets as shown in Fig. 8(a) and (b). Multiple interior crack origins also prevailed.

For $R=0.5$, eighteen specimens in total failed in the HCF and the VHCF regimes. As listed in Table 1, eleven failed from surface-with-facets and seven failed from interior-with-facets as shown in Fig. 8(c) and (d). For the case of $R=0.5$, surface-without-facets is not found.

Above all, the variation of crack initiation patterns with the increase of stress ratio is evident. With the increase of stress ratio, surface-without-facets decreased and surface-with-facets increased, whereas interior-with-facets increased first and then decreased. In other words, the increase of stress ratio together with the increase of the applied maximum stress results in the restraint of surface initiation without subsurface facets and the activation of crack interior initiation with facets. These are the experimental results of fatigue crack initiation mechanism in the HCF and the VHCF regimes for the titanium alloy, and the competition among the mechanisms will be analyzed in the next section.

3.3. Characteristic sizes of interior crack initiation region

As mentioned above, crack interior initiation occurred at the stress ratios of −0.1, 0.1 and 0.5 with the morphology of rough area as the initiation region containing a number of facets. The size of the rough area $area_{ini}^{1/2}$ and the size of facets $area_{fac}^{1/2}$ of each specimen were calculated by the square root of the relevant area. Note that the size of the initiation area (rough area) $area_{ini}^{1/2}$ includes the projection area of contained facets, and the size of

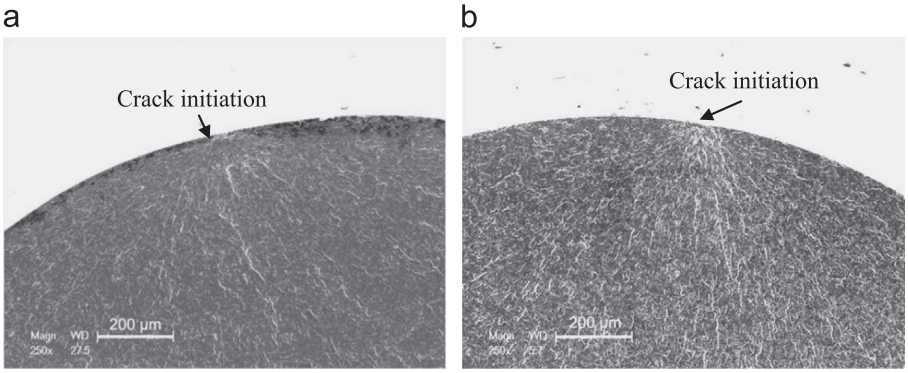

Fig. 6. Two examples of crack initiation by surface-without-facets. (a) $R=-1$ and (b) $R=-0.5$.

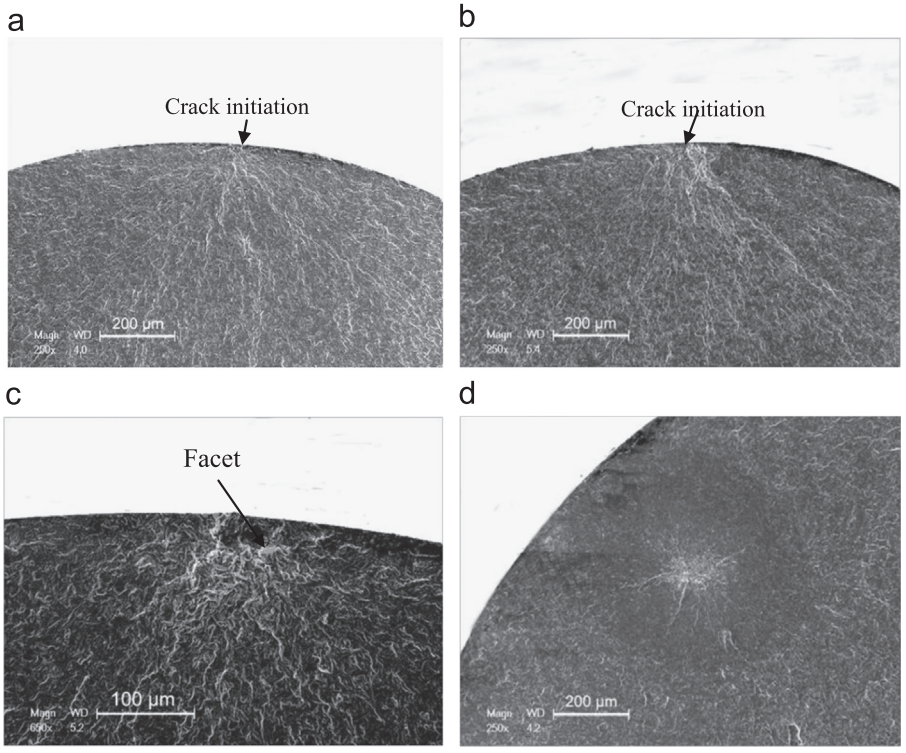

Fig. 7. Typical examples of fracture surfaces for specimens at $R=-0.1$. (a) Surface-without-facets, (b) surface-without-facets, (c) surface-with-facets, and (d) interior-with-facets.

facets $area_{fac}^{1/2}$ includes the facets within a rough area. Fig. 9 (a) presents the relationship between the size of initiation area and the fatigue life at different stress ratios. It is seen that the values of $area_{ini}^{1/2}$ increase with the increase of stress ratio and fatigue life. Fig. 9(b) presents the relationship between the size of facets $area_{fac}^{1/2}$ and the fatigue life at different stress ratios. It is seen that the values of $area_{fac}^{1/2}$ increase with the increase of stress ratio. This indicates that with the increase of stress ratio, the increase of the applied maximum stress promotes the occurrence of crack interior initiation with a pattern of rough area containing distributed facets.

4. Discussion

4.1. A model for explaining the competition of three failure types

Basically, the change of failure mode with the variation of stress ratio will cause the difference in fatigue behavior of the Ti–6Al–4V alloy. As known, the applied maximum stress dominates the occurrence of cleavage, and the applied amplitude stress dominates the process of slip deformation. The increase of stress ratio will result in the increase of $\Delta\sigma_{t,\,max}$ and the decrease of $\Delta\sigma_{t,amp}$, which leads to the occurrence of cleavage and the restraint of slip. Here, we consider the increase of the applied maximum stress as the result of the increase of stress ratio to explain the competition of failure types.

As for the three failure types of crack initiation in this investigation, first we analyze the competition of the surface-with-facets and interior-with-facets. It is noted that the fatigue strength and the fatigue life of materials are statistical and governed by defect distribution and specimen control volume [35–37], and the cleavage strength of each grain is not the same [38]. The probability density of grains for which cleavage occurs, f, follows the classical Gaussian distribution as the following equation:

$$f=\frac{1}{\sqrt{2\pi}d}e^{-\frac{(\sigma_{max}-\sigma_{c,m})^2}{2d^2}} \quad (1)$$

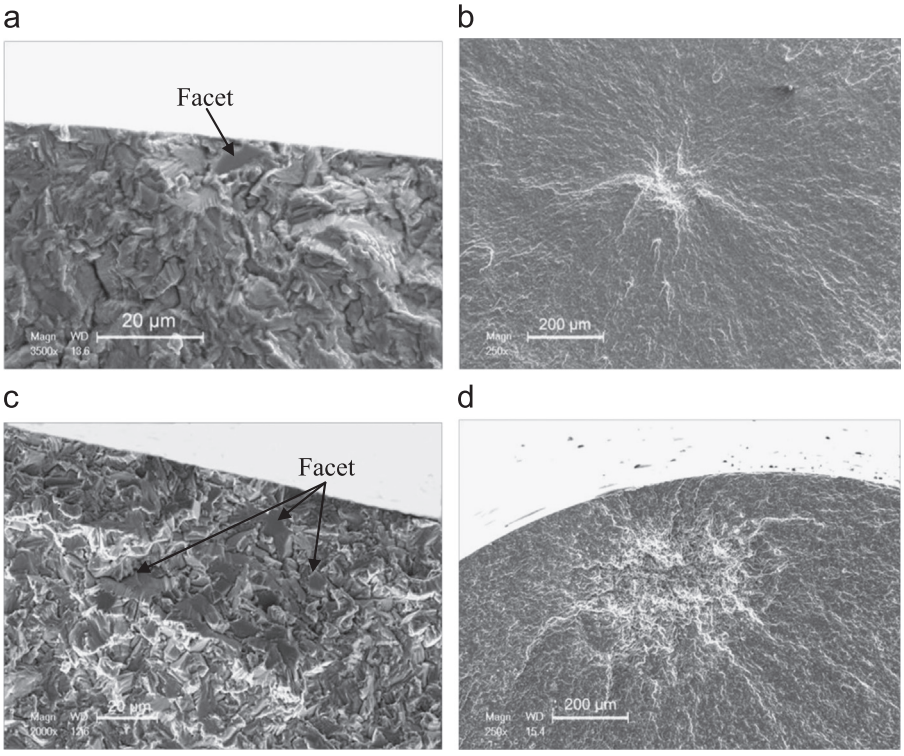

Fig. 8. Typical examples of crack initiation with facets. (a) $R=0.1$, surface-with-facets, (b) $R=0.1$, interior-with-facets, (c) $R=0.5$, surface-with-facets, and (d) $R=0.5$, interior-with-facets.

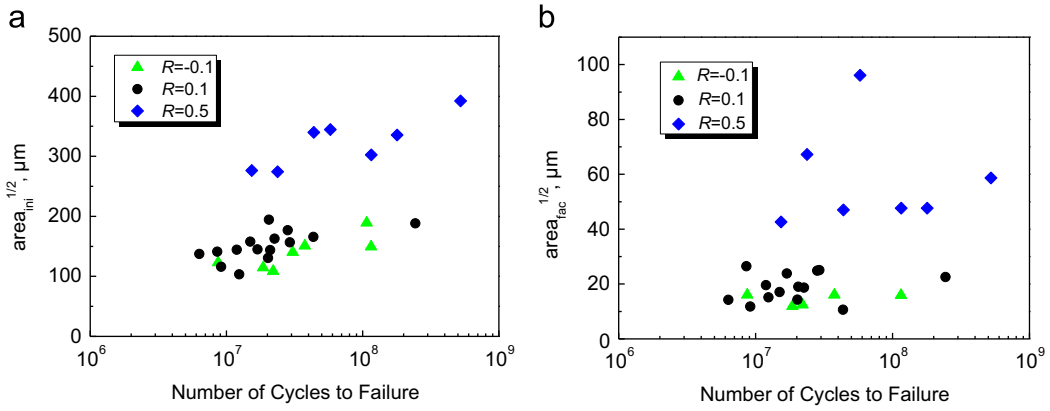

Fig. 9. (a) Size of rough area versus fatigue life for different stress ratios and (b) facet size of initiation region versus fatigue life for different stress ratios.

where σ_{max} is the applied maximum stress, $\sigma_{c,m}$ is the mean value of the cleavage strength, and d is the related variance.

The cumulative probability of grains for which cleavage occurs, F, is calculated by the integration of Eq. (1). Here, the method that the occurrence probability of the defects is determined from the two-dimensional Poisson defect distribution [6] is used in the derivation. Denote the area of the section bearing the fatigue loading as A, and the grain area of the material as a. Thus, the number of grains that may cleavage is

$$N = FA/a \tag{2}$$

Then, the Poisson distribution of occurrence probability for the number (n) of total random defects (N) in the area A is

$$P(n) = \frac{e^{-N}(N)^n}{n!} \tag{3}$$

The occurrence probabilities without activated defect $(n=0)$ and with activated defects $(n \geq 1)$ in relation to the total defects N are given by

$$P(n=0) = e^{-N} \tag{4}$$

$$P(n \geq 1) = 1 - e^{-N} \tag{5}$$

Denote A_{int} as the interior area of the cross section and A_{sur} as the surface rim area of the cross section. Then the values of activated defects that may cleavage in the total interior area N_{int} and in the total surface rim area N_{sur} are

$$N_{int} = FA_{int}/a \tag{6}$$

$$N_{sur} = FA_{sur}/a \tag{7}$$

Note that the facets initiated in the surface rim area, in comparison with that in interior area, are more prone to form a local damage region to cause crack initiation. This is due to the assumption that cracks may initiate from the surface with (subsurface) facets when there is at least one activated defect that

cleavages in the site regardless of the existence of activated defects in the interior. Therefore, the probability of surface-with-facets, P_{sur}, is

$$P_{sur} = P_{sur}(n \geq 1) = 1 - e^{-N_{sur}} \tag{8}$$

The case of interior-with-facets occurs on the condition that there is no one of activated defects in the surface rim area. The probability of interior-with-facets, P_{int}, is

$$P_{int} = P_{sur}(n = 0)P_{int}(n \geq 1) = (1 - e^{-N_{int}})e^{-N_{sur}} \tag{9}$$

Eqs. (8) and (9) are formulae expressing the competition of surface and interior initiation with facets. The proportion of the failure from surface-without-facets P_{sli} is the proportion that none of surface-with-facets, P_{sur}, and interior-with-facets, P_{int}, happens such that

$$P_{sli} = P_{sur}(n = 0)P_{int}(n = 0) = e^{-(N_{int} + N_{sur})} \tag{10}$$

The probabilities obtained by Eqs. (8)–(10) are plotted as a function of the applied maximum stress as shown in Fig. 10, where the mean stress of cleavage is taken as the tensile strength and an appropriate variance was adopted. It is seen that with the increase of the applied maximum stress, the probability of failure for surface-without-facets decreases and that for surface-with-facets increases, whereas the probability of failure for interior-with-facets increases first and then decreases. For the purpose of comparison with experiments, Fig. 11 presents the proportion of each failure type versus stress ratio in Table 1, which indicates that with the increase of the stress ratio (i.e., the increase of $\Delta\sigma_{t,\,max}$), the preference tendency for the three failure types of crack initiation given by the model in Fig. 10 is in agreement with that from the experimental results.

Here, the physical nature of the competition of the three failure types is also noticed. Apparently, the applied amplitude stress controls the fatigue failure with slip, and the applied maximum stress controls the fatigue failure with cleavage. The three failure types, surface-without-facets, surface-with-facets and interior-with-facets, are the results of the competition between two failure mechanisms, i.e., slip and cleavage. At low stress ratios, the value of $\Delta\sigma_{t,amp}$ is relatively larger than the threshold for the formation of persistent slip band (PSB), and the value of $\Delta\sigma_{t,\,max}$ is less than the threshold for the cleavage of primary α grains. Therefore, the fatigue failure mode of surface-without-facets dominates at low stress ratios. Further, due to the existence of threshold value for the formation of PSB, the fatigue strength of the Ti–6Al–4V alloy exhibits a fatigue limit, and the *S–N* curve presents the traditional asymptote shape. At high stress ratios, $\Delta\sigma_{t,amp}$ is less than the threshold for the formation of PSB, which restrains the fatigue failure with slip. Meanwhile, $\Delta\sigma_{t,\,max}$ is larger than the threshold for the cleavage of primary α grain, which triggers the fatigue failure with cleavage. In other words, the fatigue failure mode with subsurface facets or interior facets dominates at high stress ratios. In this case, the traditional fatigue limit disappears due to the occurrence of fatigue failure induced by cleavage, and the *S–N* curve presents the duplex shape.

As a consequence, the experimental revelations and the related mechanisms of different crack initiation types in the HCF and the VHCF regimes for the titanium alloy are analyzed, and the result provides a new angle to understand the raised point of the competition mechanism of fatigue crack initiation types in the HCF and the VHCF regimes for titanium alloys.

4.2. Stress intensity factor range for rough area

The crack initiation region of rough area is regarded as a crack, and the stress intensity factor range (SIF) at the tip of the rough area, ΔK_{ini}, is calculated by using the following equation [39]:

$$\Delta K_{ini} = 0.5\Delta\sigma\sqrt{\pi\sqrt{area_{ini}}} \tag{11}$$

where $\Delta\sigma$ is the stress range for $R \geq 0$ or the positive part of stress range for $R < 0$. The results are plotted as a function of fatigue life as shown in Fig. 12. It is seen that the values of ΔK_{ini} are in the range of $6-8$ MPa m$^{1/2}$ regardless of fatigue lifetime and stress ratio. The mean value of the ΔK_{ini} is 7.0 MPa m$^{1/2}$, which approximates to the value of the threshold for crack growth (7.8 MPa m$^{1/2}$) in vacuum [23]. We also calculated the values of ΔK_{ini} from the

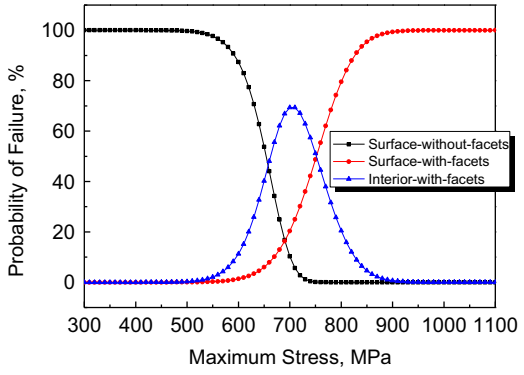

Fig. 10. Calculated probabilities for the three failure types as a function of the applied maximum stress.

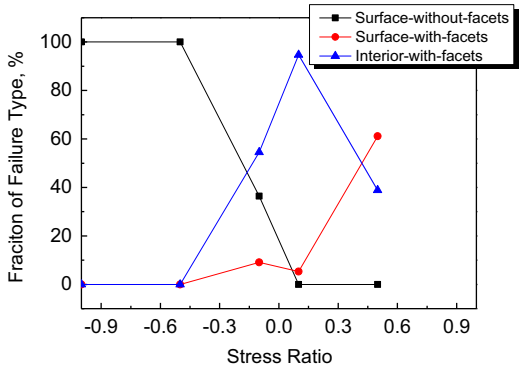

Fig. 11. Fraction of failure type as a function of stress ratio.

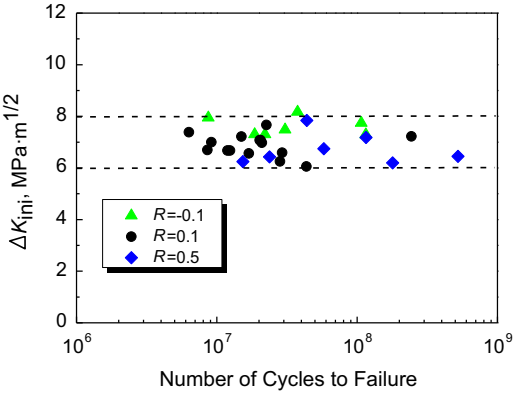

Fig. 12. Relationship between SIF range and fatigue life.

experimental data available in literature, which are 6.6 and 7.3 MPa $m^{1/2}$ [20], 6.1 and 6.7 [21], and 5.9 MPa $m^{1/2}$ [22]. From the above discussion, the value of SIF at the tip of crack initiation region (ΔK_{ini}) is close to the threshold for a crack to grow in vacuum for the material.

The model for the formation of FGA based on the plastic zone at crack tip can be referred [32,40]. During the crack initiation and early growth, a short crack is affected by the microstructure: when the plastic zone size of a crack is less than the characteristic size of the material, the fatigue crack growth rate will be greatly influenced by the microstructure orientation and shows great scattering due to a fatigue crack is more prone to growth towards the most preferred direction for propagation. This may result in the formation of the rough surface area in the crack initiation region.

For mode-I crack, the plastic zone size r_p at the crack tip under plane strain condition is [41]

$$r_p = \frac{(1-2\nu)^2}{\pi}\left(\frac{\Delta K}{\sigma_y}\right)^2 \approx \frac{1}{6\pi}\left(\frac{\Delta K}{\sigma_y}\right)^2 \quad (12)$$

where ν is the Poisson ratio and σ_y is the yield strength.

The stress state of the interior initiation crack, i.e., rough area, is regarded as plane strain condition. Thus, the size of the plastic zone for each rough area is calculated by Eq. (12) and the average value is 3.94 μm, which is close to the average diameter of primary α grains (5.89 μm). This suggests that the size of α grain of the titanium alloy is a characteristic size for crack initiation.

5. Conclusions

This paper systematically investigates the effects of stress ratio on the fatigue behavior of a Ti–6Al–4V alloy in the HCF and the VHCF regimes. The following conclusions are drawn.

(1) For stress ratios of −1 and −0.5, the *S–N* curves present a horizontal asymptote shape and have a fatigue limit. For the stress ratios of −0.1, 0.1 and 0.5, the *S–N* curves present a stepwise or duplex shape. The fatigue strength exhibits a sharp decrease between fatigue life of 10^6 and 10^9 cycles. The *S–N* curve switching from the asymptote shape to the duplex shape is attributed to the change of failure type of crack initiation.

(2) Three failure types of fatigue crack initiations are revealed and explicitly classified as surface-without facets, surface-with-facets and interior-with-facets. The occurrence preference of failure type is identified to be related to the state of stress ratio. With the increase of stress ratio, the number of specimens for surface-without-facets decreases, that for surface-with-facets increases, and that for interior-with-facets increases first and then decreases.

(3) A new model based on the Poisson defect distribution is proposed to describe the competition mechanism among the three failure types of the titanium alloy in the HCF and the VHCF regimes with the increase of the applied maximum stress, i.e., with the increase of stress ratio, which is in agreement with experimental results.

(4) The values of the stress intensity factor range for crack initiation region are within a small range of 6–8 MPa $m^{1/2}$, which are independent of the stress ratio and the fatigue life and close to the threshold value of crack growth in vacuum for the material. The average value of the plastic zone size at the front of the crack initiation region is 3.94 μm, which is close to the average diameter of primary α grains.

Acknowledgments

The financial supports by the National Basic Research Program of China (2012CB937500) and by the National Natural Science Foundation of China (11202210, 11172304 and 11021262) are gratefully appreciated.

References

[1] J.C. Williams, E.A. Starke, Acta Mater. 51 (2003) 5775–5799.
[2] A.A. Shanyavskiy, Sci. China-Phys. Mech. Astron. 57 (2014) 19–29.
[3] F.D. Neal, P.A. Blenkinsop, Acta Metall. 24 (1976) 59–63.
[4] C.J. Szczepanski, S.K. Jha, J.M. Larsen, J.W. Jones, Metall. Mater. Trans. A 39 (2008) 2841–2851.
[5] K. Tokaji, H. Kariya, Mater. Sci. Eng. A 281 (2000) 268–274.
[6] K.S. Ravi Chandran, S.K. Jha, Acta Mater. 53 (2005) 1867–1881.
[7] K.S. Ravi Chandran, P. Chang, G.T. Cashman, Int. J. Fatigue 32 (2010) 482–491.
[8] S.K. Jha, K.S. Ravi Chandran, Scr. Mater. 48 (2003) 1207–1212.
[9] K.S.R. Chandran, Nat. Mater. 4 (2005) 303–308.
[10] S.Q. Wang, J.H. Liu, Z.X. Lu, D.L. Chen, Mater. Sci. Eng. A 598 (2014) 122–134.
[11] C.Q. Sun, Z.Q. Lei, Y.S. Hong, Mech. Mater. 69 (2014) 227–236.
[12] K.F. Walker, J.C. Newman, Fatigue Fract. Eng. Mater. Struct. 37 (2014) 659–670.
[13] Y. Ji, S. Wu, G. Yu, Fatigue Fract. Eng. Mater. Struct. 37 (2014) 39–49.
[14] Z.Y. Huang, Q.Y. Wang, D. Wagner, C. Bathias, J.L. Chaboche, Fatigue Fract. Eng. Mater. Struct. 36 (2013) 462–468.
[15] Z.Y. Huang, D. Wagner, Q.Y. Wang, C. Bathias, Mater. Sci. Eng. A 559 (2013) 790–797.
[16] G. Olmi, A. Freddi, Fatigue Fract. Eng. Mater. Struct. 36 (2013) 981–993.
[17] S. Stanzl-Tschegg, Int. J. Fatigue 28 (2006) 1456–1464.
[18] H. Mayer, B. Holper, B. Zettl, S.E. Stanzl-Tschegg, Z. Metallkde 94 (2003) 539–546.
[19] R. Morrissey, T. Nicholas, Int. J. Fatigue 28 (2006) 1577–1582.
[20] J.H. Zuo, Z.G. Wang, E.H. Han, Mater. Sci. Eng. A 473 (2008) 147–152.
[21] E. Takeuchi, Y. Furuya, N. Nagashima, S. Matsuoka, Tetsu-to-Hagane 96 (2010) 36–41.
[22] E. Takeuchi, Y. Furuya, N. Nagashima, S. Matsuoka, Fatigue Fract. Eng. Mater. Struct. 31 (2008) 599–605.
[23] H. Oguma, T. Nakamura, Int. J. Fatigue 50 (2013) 89–93.
[24] H. Oguma, T. Nakamura, Scr. Mater. 63 (2010) 32–34.
[25] P.J. Golden, R. John, W.J. Porter, Procedia Eng. 2 (2010) 1839–1847.
[26] P.J. Golden, R. John, W.J. Porter, Int. J. Fatigue 31 (2009) 1764–1770.
[27] Y.S. Hong, Z.Q. Lei, C.Q. Sun, A.G. Zhao, Int. J. Fatigue 28 (2014) 144–151.
[28] Y.S. Hong, A.G. Zhao, G.A. Qian, C.E. Zhou, Metall. Mater. Trans. A 43 (2012) 2753–2762.
[29] Y. Murakami, Metal Fatigue: Effects of Small Defects and Nonmetallic Inclusions, second ed., Elsevier, Amsterdam, 2002.
[30] S. Stanzl-Tschegg, R. Schuller, T. Przeorski, P. Krug, Mater. Sci. Eng. A 538 (2012) 327–334.
[31] Z.Q. Lei, Y.S. Hong, J.J. Xie, C.Q. Sun, A.G. Zhao, Mater. Sci. Eng. A 558 (2012) 234–241.
[32] A.G. Zhao, J.J. Xie, C.Q. Sun, Z.Q. Lei, Y.S. Hong, Mater. Sci. Eng. A 528 (2011) 6872–6877.
[33] O. Takeshi, S. Stanzl-Tschegg, B.M. Schoenbauer, Eng. Fract. Mech. 115 (2014) 241–254.
[34] S. Kazuaki, K. Yasushi, N. Seiichi, Tetsu-to-Hagane 64 (1998) 94–101.
[35] Z.Q. Lei, J.J. Xie, C.Q. Sun, Y.S. Hong, Sci. China-Phys. Mech. Astron. 57 (2014) 74–82.
[36] A.M. Freudenthal, Proc. R. Soc. A 187 (1946) 416–429.
[37] F. Berto, P. Lazzarin, Sci. China-Phys. Mech. Astron. 57 (2014) 30–38.
[38] D.M. Sparkman, H.R. Millwater, S. Ghosh, Fatigue Fract. Eng. Mater. Struct. 36 (2013) 994–1008.
[39] Y. Murakami, S. Kodama, S. Konuma, Trans. Jpn. Soc. Mech. Eng. 54 (1988) 688–695.
[40] A.G. Zhao, J.J. Xie, C.Q. Sun, Z.Q. Lei, Y.S. Hong, Int. J. Fatigue 38 (2012) 46–56.
[41] R.W. Hertzberg, R.P. Vinci, J.L. Hertzberg, Deformation and Fracture Mechanics of Engineering Materials, fifth ed., Wiley, Hoboken, 2012.